

Spatially-Adaptive Feature Modulation for Efficient Image Super-Resolution

Long Sun, Jiangxin Dong, Jinhui Tang, Jinshan Pan
Nanjing University of Science and Technology

Abstract

Although numerous solutions have been proposed for image super-resolution, they are usually incompatible with low-power devices with many computational and memory constraints. In this paper, we address this problem by proposing a simple yet effective deep network to solve image super-resolution efficiently. In detail, we develop a spatially-adaptive feature modulation (SAFM) mechanism upon a vision transformer (ViT)-like block. Within it, we first apply the SAFM block over input features to dynamically select representative feature representations. As the SAFM block processes the input features from a long-range perspective, we further introduce a convolutional channel mixer (CCM) to simultaneously extract local contextual information and perform channel mixing. Extensive experimental results show that the proposed method is $3\times$ smaller than state-of-the-art efficient SR methods, e.g., IMDN, in terms of the network parameters and requires less computational cost while achieving comparable performance. The code is available at <https://github.com/sunny2109/SAFMN>.

1. Introduction

Single image super-resolution (SISR) aims to restore a high-resolution (HR) image from its low-resolution (LR) counterpart by recovering lost details. This longstanding and challenging task has recently attracted much attention due to the rapid development of streaming media or high-definition devices. As these scenarios are usually resource-constrained, it is of great interest to develop an efficient and effective SR method to estimate HR images for better visual display on these platforms or products.

Deep learning-based SR methods have achieved significant performance improvements with the great evolution of hardware technologies, as we can use large amounts of data to train much larger or deeper neural networks for image SR [5, 30, 31, 50]. For example, RCAN [50] is a representative CNN-based image SR network with 15.59M parameters and reaching a depth of over 400 layers. One of the most significant drawbacks of these large models is that they require high computational costs, which makes them

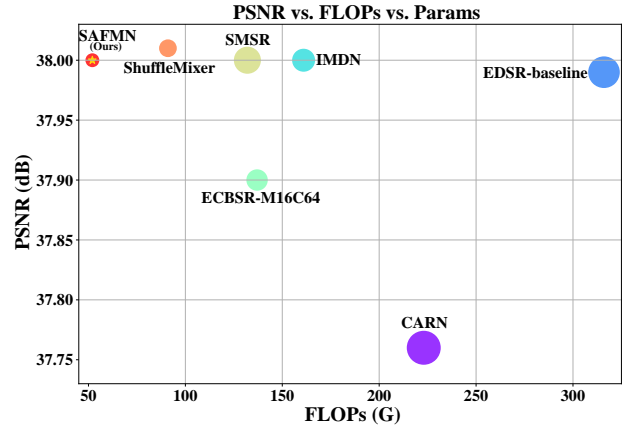


Figure 1. Model complexity and performance comparison between our proposed SAFMN model and other lightweight methods on Set5 [4] for $\times 2$ SR. Circle sizes indicate the number of parameters. The proposed method achieves a better trade-off between model complexity and reconstruction performance.

challenging to deploy. Moreover, recent visual transformers (ViTs) [5, 11, 30] well beyond convolutional neural networks (CNNs) in low-level vision tasks, and their results demonstrate that exploring non-local feature interactions is essential for high-quality reconstruction. But existing self-attention mechanisms are computationally expensive and unfriendly to efficient SR design. This, therefore, motivates us to develop a lightweight yet effective model for real-world applications of image super-resolution by integrating the principles of convolution and self-attention.

To reduce the heavy computational burden, various methods, including efficient module design [1, 10, 19, 25, 29, 32, 36, 41, 51], knowledge distillation [15], neural architecture search [6, 40], and structural re-parameterization [49], are trying to improve the efficiency of SR algorithms. Among these efficient SR models, one direction is to reduce model parameters or complexity (FLOPs). Lightweight strategies like recursive manner [22, 42], parameter sharing [1], and sparse convolutions [1, 29, 41] are adopted. Although these approaches certainly reduce the model size, they usually compensate for the performance drop caused by shared recursive modules or sparse convolutions by increasing the depth or width of the model, which affects the inference efficiency when performing SR reconstruction.

Another direction is to accelerate the inference time. The post-upsampling [10, 39] is an important replacement for the pre-defined input [9, 23], which significantly speeds up the runtime. Model quantization [20] effectively accelerates latency and reduces energy consumption, particularly when deploying algorithms in edge-devices. Structural re-parameterization [7, 49] improves the speed of a well-trained model in the inference stage. These methods enjoy fast running time but poor reconstruction performance. Consequently, there is still room for a better trade-off between model efficiency and reconstruction performance.

To address the above-mentioned issues, we design a simple yet effective model by developing a spatially-adaptive feature modulation, namely SAFMN, to realize a favorable trade-off between performance and efficiency. Different from stacking lightweight convolutional modules, we explore a ViT-like architecture for better modeling long-range feature relations, as depicted in Figure 2. Specifically, we develop a multi-scale representation-based feature modulation mechanism to dynamically select representative features. Since the modulation mechanism processes input features from a long-range perspective, there is a requirement to complement local contextual information. To this end, we present a convolutional channel mixer based on FMB-Conv [43] to encode local features and mix channels simultaneously. Taken together, we find that the SAFMN network is able to achieve a better trade-off between SR performance and model complexity, as shown in Figure 1.

The main contributions of this paper are summarized as follows:

- We propose a lightweight and effective SR model which absorbs CNN-like efficiency and transformer-like adaptability.
- We develop a compact convolutional channel mixer to encode local contextual information and perform channel mixing simultaneously.
- We evaluate the proposed method quantitatively and qualitatively on benchmark datasets, and the results show that our SAFMN achieves a favorable trade-off between accuracy and model complexity.

2. Related Work

Deep Learning-based Image Super-Resolution. Classical interpolation algorithms, such as linear or bicubic upsampling, create high-resolution images by inserting zeros between adjacent pixels in the low resolution and then using a low-pass filter to preserve the content information of the input image [36]. Unlike these interpolation-based upsamplers, deep learning-based approaches learn a nonlinear mapping between the input image and the target output in an end-to-end training fashion. SRCNN [9] is the first attempt to use a convolutional neural network (CNN)

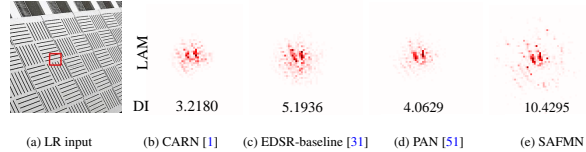


Figure 2. Comparison of local attribution maps (LAMs) [12] and diffusion indices (DIs) [12] between our SAFMN and other efficient SR models. The LAM results denote the importance of each pixel in the input LR image when super-resolving the patch marked with a red box. The DI value reflects the range of involved pixels. A larger DI value means a wider range of attention. The proposed method could exploit more feature information.

to tackle the image SR problem and achieves a considerable performance gain compared with conventional methods. Since then, many improvements have been proposed. VDSR [23] uses global residual learning [14] to solve the problem of difficulty in training an SR model with deep layers. DRRN [42] integrates the local residual learning and global residual connection to ease the training difficulty and enhance high-frequency details. EDSR [31] further increases the model footprint to 43M, achieving a significant breakthrough in reconstruction performance and showing that the BatchNorm (BN) [21] layer is not necessary for the SR task. RCAN [50] builds a more than 400 layers model based on channel attention and dense connections for accurate SR. With the successful application of ViT in various high-level vision tasks, image SR also follows this ViT [11] scheme and obtains higher performance than CNN-based models. For instance, SwinIR [30] acts as a strong baseline for image restoration tasks based on the Swin Transformer [33]. While these approaches achieve impressive reconstruction performance, the required high computational costs make them challenging to deploy in real-world applications on resource-constrained devices.

Efficient Image Super-Resolution. To improve the model efficiency, many CNN-based SR works try to alleviate this issue. FSRCNN [10] and ESPCN [39] utilize a post-upsampling manner to reduce the computational burden from the pre-defined inputs significantly. CARN [1] uses group convolutions and a cascading mechanism upon residual networks to improve efficiency. IMDN [19] adopts feature splitting and concatenation operations to progressively aggregate features, and its improved variants [25, 32] won the AIM2020 and NTIRE2022 Efficient SR challenge. ShuffleMixer [41] introduces a large kernel convolution for lightweight SR design. BSRN [29] proposes a blueprint-separable convolution-based model to reduce model complexity. Meanwhile, an increasingly popular direction is to compress or accelerate a well-trained deep model through model quantization [20], structural re-parameterization [49] or knowledge distillation [15]. Neural architecture search (NAS) is also commonly used to search a well-constrained architecture for image super-resolution [6, 40]. Note that

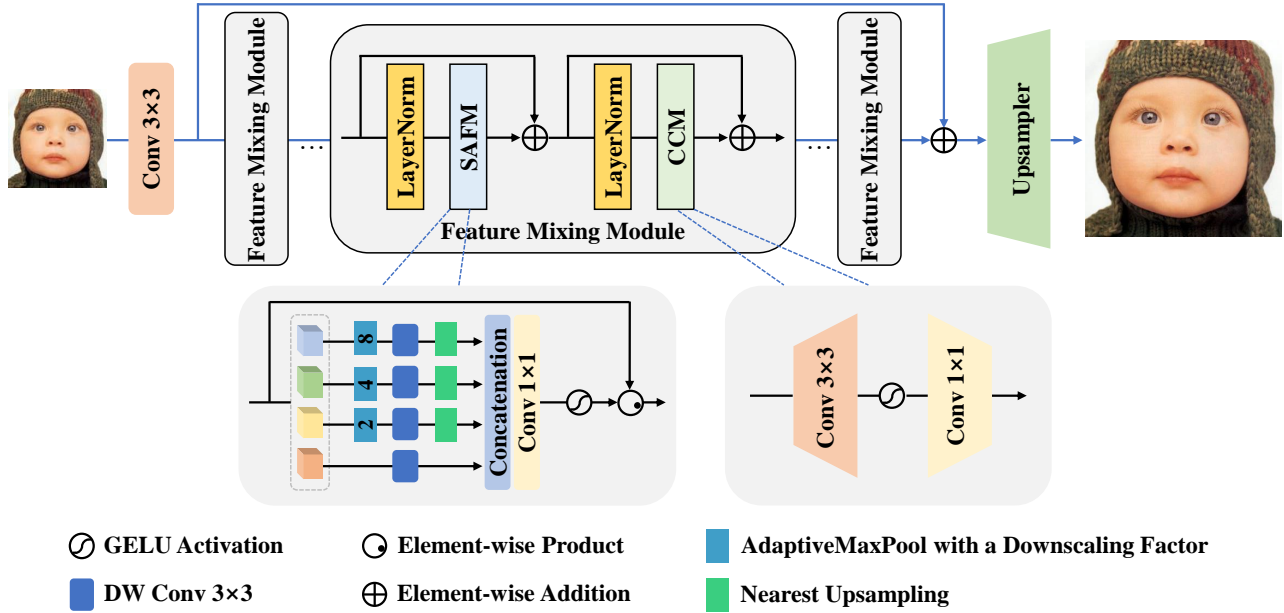


Figure 3. An overview of the proposed SAFMN. SAFMN first transforms the input LR image into the feature space using a convolutional layer, performs feature extraction using a series of feature mixing modules (FMMs), and then reconstructs these extracted features by an upsampler module. The FMM block is mainly implemented by a spatially-adaptive feature modulation (SAFM) layer and a convolutional channel mixer (CCM).

the efficiency of a deep neural network could be measured in different metrics, including the number of parameters, FLOPs, activations, memory consumption and inference running time [28, 48]. Although the above approaches have been improved in different efficiency aspects, there is still room for a favorable trade-off between reconstruction performance and model efficiency.

3. Proposed Method

In this section, we present the core components of our proposed model for efficient SISR. As shown in Figure 3, the network consists of the following parts: a stacking of feature mixing modules (FMMs) and an upsampler layer. Specifically, we first apply a convolution layer with a kernel size of 3×3 pixels to transform the input LR image to feature space and generate the shallow feature F_0 . Then, the multiple stacked FMMs are used to generate finer deep features from F_0 for HR image reconstruction, where an FMM layer has a spatially-adaptive feature modulation (SAFM) sub-layer and a convolutional channel mixer (CCM). To recover the HR target image, we introduce a global residual connection to learn high-frequency details and employ a lightweight upsampling layer for fast reconstruction, which only contains a 3×3 convolution and a sub-pixel convolution [39]. Our network can be formulated as:

$$\begin{aligned} F_0 &= \mathcal{C}_\omega(I_{LR}), \\ I_{SR} &= \mathcal{U}_\gamma(\mathcal{M}_\theta(F_0) + F_0), \end{aligned} \quad (1)$$

where I_{SR} is the predicted HR image, I_{LR} is the input LR image, $\mathcal{C}_\omega(\cdot)$ is the first convolution parameterized by ω , $\mathcal{M}_\theta(\cdot)$ denotes stacked FMM modules parameterized by θ , and $\mathcal{U}_\gamma(\cdot)$ represents the upsampler function parameterized by γ . Following the previous work [41], these parameters are optimized using a combination of mean absolute error (MAE) loss and an FFT-based frequency loss function, which is defined as:

$$\mathcal{L} = \|I_{SR} - I_{HR}\|_1 + \lambda \|\mathcal{F}(I_{SR}) - \mathcal{F}(I_{HR})\|_1, \quad (2)$$

where I_{HR} is the high-quality ground-truth image, $\|\cdot\|_1$ denotes the L_1 -norm, \mathcal{F} represents the Fast Fourier transform, and λ is a weight parameter that is set to be 0.05 empirically.

3.1. Spatially-adaptive Feature Modulation

Compared to the self-attention mechanism [11, 30, 33] or the large kernel convolution [8, 13], we propose a lightweight alternative to learn long-range dependencies from multi-scale feature representations so that more useful features can be better explored for HR image reconstruction. As shown in Figure 3, we apply a feature pyramid to generate an attention map for spatially-adaptive feature modulation. To reduce the model complexity and obtain a pyramidal feature representation, we first employ a channel split operation on the normalized input features, producing four-part components. A 3×3 depth-wise convolution processes the first one, and the rest parts are fed into a multi-

scale feature generation unit. Given the input feature X , this procedure can be expressed as:

$$\begin{aligned} [X_0, X_1, X_2, X_3] &= \text{Split}(X), \\ \hat{X}_0 &= \text{DW-Conv}_{3 \times 3}(X_0), \\ \hat{X}_i &= \uparrow_p (\text{DW-Conv}_{3 \times 3}(\downarrow_{\frac{p}{2^i}}(X_i))), 1 \leq i \leq 3, \end{aligned} \quad (3)$$

where $\text{Split}(\cdot)$ is the channel split operation, $\text{DW-Conv}_{3 \times 3}(\cdot)$ is a depth-wise convolution with a kernel size of 3×3 pixels, $\uparrow_p(\cdot)$ represents upsampling features at a specific level to the original resolution p via nearest interpolation for fast implementation, and $\downarrow_{\frac{p}{2^i}}$ denotes downsampling the input features to the size of $\frac{p}{2^i}$. As we desire to select discriminative features towards learning non-local interactions, adaptive max pooling is applied over the input features to generate multi-scale features. Results in Table 3 illustrate that this max pooling operation helps to improve reconstruction performance. We then concatenate these multi-scale features to aggregate local and global relations by a 1×1 convolution. It can be expressed by:

$$\hat{X} = \text{Conv}_{1 \times 1} \left(\text{Concat}([\hat{X}_0, \hat{X}_1, \hat{X}_2, \hat{X}_3]) \right), \quad (4)$$

where $\text{Concat}(\cdot)$ denotes a concatenation operation along the channel dimension, and $\text{Conv}_{1 \times 1}(\cdot)$ is the 1×1 convolution. After obtaining the refined representation \hat{X} , we normalize it through a GELU non-linearity [16] to estimate the attention map and adaptively modulate X according to the estimated attention in an element-wise product. This process can be written as:

$$\bar{X} = \phi(\hat{X}) \odot X, \quad (5)$$

where $\phi(\cdot)$ represents the GELU function and \odot is the element-wise product. Figure 2 and Table 2 intuitively illustrate that benefiting from the multi-scale feature representation, we can apply such a spatially-adaptive modulation mechanism for gathering long-range features with small memory and computational costs. As shown in Table 3, this multi-scale form achieves better performance with less memory consumption than directly extracting features with a depth-wise convolution.

3.2. Convolutional Channel Mixer

We note that the SAFM sub-block focuses on exploring the global information while the local contextual information also facilitates high-resolution image reconstruction. Different from the commonly used feed-forward network [11, 30, 33] that uses two consecutive 1×1 convolutions to transform the features in channel dimensions for local context information exploration, we present a convolutional channel mixer (CCM) based on the FMBCConv [43]

to enhance the local spatial modelling ability and perform channel mixing. The proposed CCM contains a 3×3 convolution and a 1×1 convolution. Within this, the first 3×3 convolution encodes the spatially local contexts and **doubles** the number of channels of the input features for mixing channels; the later 1×1 convolution reduces the channels back to the original input dimension. A GELU [16] function is applied to the hidden layer for non-linear mapping. This manner is more memory-efficient than employing a 3×3 depth-wise convolution on the extended dimension (e.g. Inverted residual block [38]), as shown in Table 3. Compared with the original FMBCConv, we made the following modifications to make it more compatible with our architecture: (1) removing the squeeze-and-excitation (SE) block [17]; (2) replacing the BatchNorm [21] with the LayerNorm [3] and moving it before the convolution. Excluding the SE block mainly because the SAFM also has a dynamic utility on the channel dimension, and the reconstruction performance does not drop without it. In addition, using the LayerNorm enables better stabilization of the model training and better results, as discussed in Section 5.

3.3. Feature Mixing Module

Motivated by the network design of ViT that contains a self-attention module for global feature aggregation and a feed-forward network for feature refinement, we formulate the proposed SAFM and the CCM into a unified feature mixing module to select representative features. The feature mixing module can be formulated as:

$$\begin{aligned} Y &= \text{SAFM}(\text{LN}(X)) + X, \\ Z &= \text{CCM}(\text{LN}(Y)) + Y, \end{aligned} \quad (6)$$

where $\text{LN}(\cdot)$ is the LayerNorm [3] layer, X , Y , and Z are the intermediate features.

4. Experimental Results

In this section, we perform quantitative and qualitative evaluations to demonstrate the effectiveness of the proposed method.

4.1. Dataset and Implementation

Datasets. Following previous works [27, 30, 41], we use DIV2K [44] and Flickr2K [31] as the training data and generate LR images by applying the bicubic downscaling to reference HR images. We use five commonly used benchmark datasets including Set5 [4], Set14 [46], B100 [2], Urban100 [18] and Manga109 [35] as test data. We use the peak signal to noise ratio (PSNR) and the structural similarity index (SSIM) to evaluate the quality of the restored images. All PSNR and SSIM values are calculated on the Y channel of images transformed to YCbCr color space.

Table 1. **Comparisons of efficient SR networks on the commonly used benchmark datasets.** All PSNR/SSIM results are calculated on the Y-channel. #Acts represents all elements of the output of convolutional layers. #FLOPs and #Acts are measured corresponding to an HR image of the size 1280×720 pixels. **Red** color denotes the best performance. Blanked entries indicate results not reported or not available from previous work. * denotes that the results are obtained with the structural re-parameterization technique.

Methods	Scale	#Params [K]	#FLOPs [G]	#Acts [M]	Set5	Set14	B100	Urban100	Manga109
Bicubic		-	-	-	33.66/0.9299	30.24/0.8688	29.56/0.8431	26.88/0.8403	30.80/0.9339
SRCNN [9]		57	53	89	36.66/0.9542	32.42/0.9063	31.36/0.8879	29.50/0.8946	35.74/0.9661
FSRCNN [10]		12	6	41	37.00/0.9558	32.63/0.9088	31.53/0.8920	29.88/0.9020	36.67/0.9694
ESPCN [39]		21	5	23	36.83/0.9564	32.40/0.9096	31.29/0.8917	29.48/0.8975	-
VDSR [23]		665	613	1,120	37.53/0.9587	33.03/0.9124	31.90/0.8960	30.76/0.9140	37.22/0.9729
LapSRN [26]		813	30	223	37.52/0.9590	33.08/0.9130	31.80/0.8950	30.41/0.9100	37.27/0.9740
CARN-M [1]		415	91	655	37.53/0.9583	33.26/0.9141	31.92/0.8960	31.23/0.9193	-
CARN [1]		1,592	223	522	37.76/0.9590	33.52/0.9166	32.09/0.8978	31.92/0.9256	-
EDSR-baseline [31]	×2	1,370	316	563	37.99/0.9604	33.57/0.9175	32.16/0.8994	31.98/0.9272	38.54/0.9769
IMDN [19]		694	161	423	38.00/0.9605	33.63/0.9177	32.19/0.8996	32.17/0.9283	38.88/0.9774
PAN [51]		261	71	677	38.00/0.9605	33.59/0.9181	32.18/0.8997	32.01/0.9273	38.70/0.9773
LAPAR-A [27]		548	171	656	38.01/0.9605	33.62/0.9183	32.19/0.8999	32.10/0.9283	38.67/0.9772
ECBSR-M16C64 [49]		596	137	252*	37.90/0.9615	33.34/0.9178	32.10/0.9018	31.71/0.9250	-
SMSR [45]		985	132	-	38.00/0.9601	33.64/0.9179	32.17/0.8990	32.19/0.9284	38.76/0.9771
ShuffleMixer [41]		394	91	832	38.01/0.9606	33.63/0.9180	32.17/0.8995	31.89/0.9257	38.83/0.9774
SAFMN		228	52	299	38.00/0.9605	33.54/0.9177	32.16/0.8995	31.84/0.9256	38.71/0.9771
Bicubic		-	-	-	30.39/0.8682	27.55/0.7742	27.21/0.7385	24.46/0.7349	26.95/0.8556
SRCNN [9]		57	53	89	32.75/0.9090	29.28/0.8209	28.41/0.7863	26.24/0.7989	30.59/0.9107
FSRCNN [10]		12	5	19	33.16/0.9140	29.43/0.8242	28.53/0.7910	26.43/0.8080	30.98/0.9212
VDSR [23]		665	613	1,120	33.66/0.9213	29.77/0.8314	28.82/0.7976	27.14/0.8279	32.01/0.9310
CARN-M [1]		415	46	327	33.99/0.9236	30.08/0.8367	28.91/0.8000	27.55/0.8385	-
CARN [1]		1,592	119	268	34.29/0.9255	30.29/0.8407	29.06/0.8034	28.06/0.8493	-
EDSR-baseline [31]	×3	1,555	160	285	34.37/0.9270	30.28/0.8417	29.09/0.8052	28.15/0.8527	33.45/0.9439
IMDN [19]		703	72	190	34.36/0.9270	30.32/0.8417	29.09/0.8046	28.17/0.8519	33.61/0.9445
PAN [51]		261	39	340	34.40/0.9271	30.36/0.8423	29.11/0.8050	28.11/0.8511	33.61/0.9448
LAPAR-A [27]		594	114	505	34.36/0.9267	30.34/0.8421	29.11/0.8054	28.15/0.8523	33.51/0.9441
SMSR [45]		993	68	-	34.40/0.9270	30.33/0.8412	29.10/0.8050	28.25/0.8536	33.68/0.9445
ShuffleMixer [41]		415	43	404	34.40/0.9272	30.37/0.8423	29.12/0.8051	28.08/0.8498	33.69/0.9448
SAFMN		233	23	134	34.34/0.9267	30.33/0.8418	29.08/0.8048	27.95/0.8474	33.52/0.9437
Bicubic		-	-	-	28.42/0.8104	26.00/0.7027	25.96/0.6675	23.14/0.6577	24.89/0.7866
SRCNN [9]		57	53	89	30.48/0.8628	27.49/0.7503	26.90/0.7101	24.52/0.7221	27.66/0.8505
FSRCNN [10]		12	5	11	30.71/0.8657	27.59/0.7535	26.98/0.7150	24.62/0.7280	27.90/0.8517
ESPCN [39]		25	1	6	30.52/0.8697	27.42/0.7606	26.87/0.7216	24.39/0.7241	-
VDSR [23]		665	613	1,120	31.35/0.8838	28.01/0.7674	27.29/0.7251	25.18/0.7524	28.83/0.8809
LapSRN [26]		813	149	264	31.54/0.8850	28.19/0.7720	27.32/0.7280	25.21/0.7560	29.09/0.8845
CARN-M [1]		415	33	227	31.92/0.8903	28.42/0.7762	27.44/0.7304	25.62/0.7694	-
CARN [1]		1,592	91	194	32.13/0.8937	28.60/0.7806	27.58/0.7349	26.07/0.7837	-
EDSR-baseline [31]	×4	1,518	114	202	32.09/0.8938	28.58/0.7813	27.57/0.7357	26.04/0.7849	30.35/0.9067
IMDN [19]		715	41	108	32.21/0.8948	28.58/0.7811	27.56/0.7353	26.04/0.7838	30.45/0.9075
PAN [51]		261	22	191	32.13/0.8948	28.61/0.7822	27.59/0.7363	26.11/0.7854	30.51/0.9095
LAPAR-A [27]		659	94	452	32.15/0.8944	28.61/0.7818	27.61/0.7366	26.14/0.7871	30.42/0.9074
ECBSR-M16C64 [49]		603	35	64*	31.92/0.8946	28.34/0.7817	27.48/0.7393	25.81/0.7773	-
SMSR [45]		1006	42	-	32.12/0.8932	28.55/0.7808	27.55/0.7351	26.11/0.7868	30.54/0.9085
ShuffleMixer [41]		411	28	269	32.21/0.8953	28.66/0.7827	27.61/0.7366	26.08/0.7835	30.65/0.9093
SAFMN		240	14	77	32.18/0.8948	28.60/0.7813	27.58/0.7359	25.97/0.7809	30.43/0.9063

Implementation details. During the training, the data augmentation is performed on the input patches with random horizontal flips and rotations. In addition, we randomly crop 64 patches of size 64×64 pixels from LR images as the basic training inputs. The number of FMM and feature channels is set to 8 and 36, respectively. We use the Adam [24] optimizer with $\beta_1 = 0.9$ and $\beta_2 = 0.99$ to solve the proposed model. The number of iterations is set to 500,000. We set the initial learning rate to 1×10^{-3} and the minimum one to 1×10^{-5} , which is updated by the Cosine Annealing scheme [34]. All experiments are conducted with the PyTorch framework on an NVIDIA GeForce RTX

3090 GPU. Due to the page limit, we include more results in the supplemental material. The training code and models will be available to the public.

4.2. Comparisons with State-of-the-Art Methods

Quantitative comparisons. To evaluate the performance of our approach, we compare it with state-of-the-art lightweight SR methods, including SRCNN [9], FSRCNN [10], ESPCN [39], VDSR [23], LapSRN [26], CARN [1], EDSR-baseline [31], IMDN [19], PAN [51], LAPAR [27], ECBSR [49], SMSR [45], and ShuffleMixer [41].

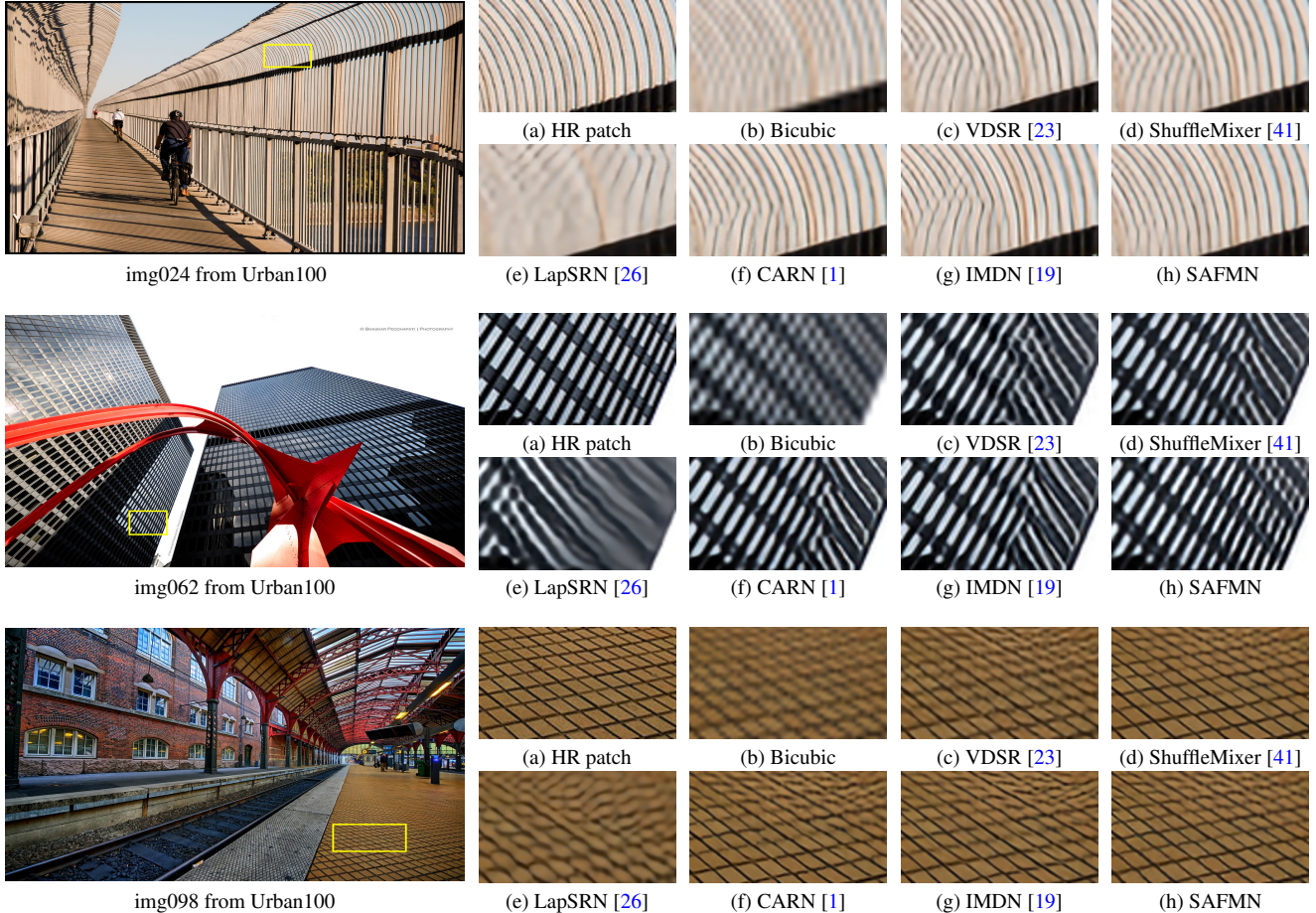


Figure 4. Visual comparisons for $\times 3$ SR on the Urban100 dataset. The proposed method recovers the image with clearer structures.

The quantitative comparisons on benchmark datasets for the upscaling factors of $\times 2$, $\times 3$, and $\times 4$ are reported in Table 1. In addition to PSNR/SSIM metrics, we list the number of parameters (#Params), FLOPs (#FLOPs) and activations (#Acts). We calculate the number of FLOPs and activations with the `fvcore`¹ library under a setting of super-resolving an LR image to 1280×720 pixels. Among these metrics, #Params and #Acts are linked to memory consumption, and #FLOPs is related to energy usage. In particular, #Acts is a better metric for measuring the efficiency of a model than the number of parameters and FLOPs as suggested in recent works [28, 37, 47, 48].

Benefiting from the simple yet efficient structure, the proposed SAFMN obtains comparable performance with significantly fewer parameters and memory consumption. Take $\times 4$ SR on B100 dataset as an example, our SAFMN has parameters about 85% less than the CARN [1], 66% less than the IMDN [19], and 42% less than the ShuffleMixer [41]. As for activations, we have 60%, 29% and 71% fewer than them, respectively. While our model has

¹We use the `fvcore.nn.flop_count_str` command to calculate the number of parameters, FLOPs and activations.

a smaller footprint, we achieve similar performance among these methods. Moreover, we compare the reconstruction accuracy, FLOPs and parameters on the $\times 2$ Set5 dataset in Figure 1. The proposed SAFMN model achieves a favorable trade-off between model complexity and reconstruction performance.

Qualitative comparisons. In addition to the quantitative evaluations, we provide qualitative comparisons of the proposed method. Figure 4 shows the visual comparisons on the Urban100 dataset for $\times 3$ SR. Our approach generates parallel straight lines and grid patterns more accurately than the listed methods. These results also demonstrate the effectiveness of our method for adaptive feature modulation by exploiting non-local feature interactions.

Memory and running time comparisons. To fully examine the efficiency of our proposed method, we further evaluate our method against five representative ones, including CARN-M [1], CARN [1], EDSR-baseline [31], IMDN [19], and LAPAR-A [27] on $\times 4$ SR in terms of the GPU memory consumption (#GPU Mem.) and running time (#Avg. Time). The maximum GPU memory consumption is recorded during the inference. The running time is

Table 2. **Memory and running time comparisons on $\times 4$ SR.** #GPU Mem. denotes the maximum GPU memory consumption during the inference phase, derived with the Pytorch `torch.cuda.max_memory_allocated()` function. #Avg. Time is the average running time on 50 LR images with a size of 320×180 pixels.

Methods	#GPU Mem. [M]	#Avg.Time [ms]
CARN-M [1]	680.84	17.85
CARN [1]	689.83	18.90
EDSR-baseline [31]	486.58	19.81
IMDN [19]	203.44	10.22
LAPAR-A [27]	1811.47	24.91
SAFMN	65.26	10.71

averaged on 50 test images with a 320×180 resolution. We show the memory and running time comparisons in Table 2, our method achieves a clear improvement over other state-of-the-art methods. By using the multi-scale modulation layer and the efficient channel mixer, the GPU consumption of our SAFMN is only 10% of the CARN series and 4% of LAPAR-A; the running time is nearly twice as fast as other evaluated methods, except for IMDN. Compared to IMDN [19], our method has a similar running time speed while significantly reducing memory usage. Tables 1 and 2 show that the proposed model achieves a favorable trade-off in terms of inference speed, model complexity and reconstruction performance against state-of-the-art methods.

5. Analysis and Discussion

We further conduct extensive ablation studies to better understand and evaluate each component in the proposed SAFMN. For fair comparisons with the designed baselines, we implement all experiments based on $\times 4$ SAFMN and train them with the same setting. The experimental results in Table 3 are measured on DIV2K-val [44] and Manga109 [35] datasets.

Effectiveness of the spatially-adaptive feature modulation. To demonstrate the effect of the spatially-adaptive feature modulation, we first remove this module for comparison. Without it, the PSNR values will drop by 0.17dB (30.26 vs. 30.43) and 0.34dB (30.09 vs. 30.43) on the DIV2K-val and Manga109 datasets, respectively. These results show the importance of the SAFM. Therefore, we further investigate this module to find out why it works.

- **Feature modulation.** The feature modulation mechanism is introduced to enable the network with adaptive properties. Without this operation, the baseline model is lowered by 0.11dB on the Manga109 dataset.
- **Multi-scale representation.** Here, “w/o MR” in Table 3 denotes that we directly use a depth-wise convolution with a kernel size of 3×3 pixels to extract spatial information and do not employ multi-scale features. A noticeable performance drop of 0.13dB on

the Manga109 dataset is observed without these multi-scale features. Moreover, we apply the adaptive max pooling over the input features in this module to build feature pyramids. Compared to using adaptive average pooling or nearest interpolation, adaptive max pooling allows the model to detect discriminative features, resulting in better reconstruction results.

- **Feature aggregation.** We use a 1×1 convolution to aggregate the multi-scale features on the channel dimension. Combined with the modulation mechanism, it brings a PSNR improvement of 0.14dB on the Manga109 dataset, which proves the necessity of aggregating the multi-scale features.

Without all three components mentioned before, it represents that only a 3×3 depth-wise convolution is used to encode the spatial information and leads to a PSNR reduction of 0.12dB and 0.2dB on the DIV2K-val and Manga109 datasets, respectively. This performance drop suggests that the spatially-adaptive modulation based on the multi-scale feature representation effectively boosts SR reconstruction performance.

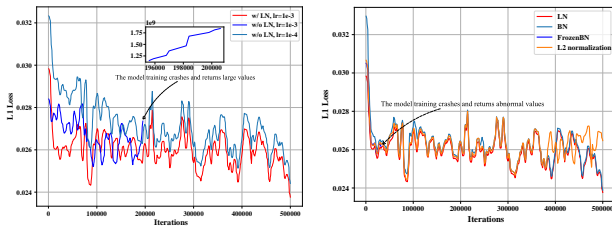
- **GELU function.** Here, we use the GELU [16] function to normalize the modulation map. Table 3 shows that better experimental results can be achieved with GELU than with Sigmoid or without GELU, mainly because it weights the input features by their percentile and allows better-activated features.

The above analysis shows that benefiting from the multi-scale feature representation, the proposed SAFM can effectively exploit long-range interactions.

Effectiveness of the convolutional channel mixer. Compared with the original FMBCConv [43], the main change made by CCM is removing the SE [17] block. As shown in Table 3, using SE blocks, its performance is almost the same as without them. This result is mainly caused by the SAFM block already performing dynamic channel-wise feature recalibration. Hence, we do not use the SE blocks for saving parameters. We next conduct a series of ablations to verify that CCM can effectively encode local contextual information and perform channel mixing. Without it, the model only achieves the accuracy of 29.69dB and 28.49dB on DIV2K-val and Manga109 datasets, proving the indispensability and locality modelling ability of this part. We then change CCM to other channel mixers commonly used in ViT architectures: channel MLP [11] or inverted residual block [38]. When the channel MLP is adopted for the channel mixer, there is a significant performance drop of 0.63dB (29.80 vs. 30.43) on the Manga109 dataset. This performance drop results from the lack of local spatial modelling ability. For the inverted residual block, the performance is highly similar to that of CCM, but the corresponding #Acts is increased by nearly 35M, which means more memory

Table 3. **Ablation for SAFMN on DIV2K-val and Manga109 datasets.** SAFMN with a scaling factor of $\times 4$ is utilized as the baseline for ablation studies. The PSNR/SSIM values on benchmarks are reported. “A \rightarrow B” is to replace A with B. “None” means to remove the operation. “lr” denotes the learning rate. “FBN” is the abbreviation of the Frozen BatchNorm. “L₂ normalization” represents that the inputs are normalized by L₂-norm over the channel dimension. “FM”, “MR”, and “FA” are the abbreviations corresponding to feature modulation, multi-scale representation, and feature aggregation. * indicates that the corresponding results are obtained before the training collapse. The numbers of parameters, #FLOPs and #Acts are counted by the fvcure library with a resolution of 320×180 pixels.

Ablation	Variant	#Params [K]	#FLOPs [G]	#Acts [M]	DIV2K-val	Manga109
Baseline	-	239.52	13.56	76.70	30.43/0.8372	30.43/0.9063
Main module	SAFM \rightarrow None	225.41	12.90	54.61	30.26/0.8330	30.09/0.9018
	CCM \rightarrow None	30.72	1.61	26.93	29.69/0.8193	28.49/0.8193
SAFM	(a): w/o FM	239.52	13.56	76.70	30.36/0.8357	30.32/0.9048
	(b): w/o MR	239.52	13.64	87.78	30.34/0.8350	30.30/0.9047
	(c): w/o FA	228.86	12.96	60.11	30.36/0.8355	30.29/0.9049
	(a) + (b)	239.52	13.64	87.78	30.32/0.8345	30.24/0.9038
	(a) + (c)	228.86	12.96	60.11	30.34/0.8351	30.28/0.9043
	(a) + (b) + (c)	228.86	13.05	71.19	30.31/0.8344	30.23/0.9036
	AdaptiveMaxPool \rightarrow AdaptiveAvgPool	239.52	13.56	76.70	30.40/0.8364	30.40/0.9061
	AdaptiveMaxPool \rightarrow Nearest interpolate	239.52	13.56	76.70	30.36/0.8354	30.31/0.9048
	GELU \rightarrow None	239.52	13.56	76.70	30.40/0.8366	30.37/0.9058
GELU \rightarrow Sigmoid	239.52	13.56	76.70	30.35/0.8355	30.29/0.9044	
CCM	w/ SE	260.98	13.59	76.70	30.39/0.8360	30.46/0.9067
	CCM \rightarrow Channel MLP	73.63	4.00	76.70	30.17/0.8313	29.80/0.8980
	CCM \rightarrow Inverted residual block	245.28	13.85	110.00	30.43/0.8373	30.43/0.9064
Normalization	LN \rightarrow None, lr= 1×10^{-3} *	238.37	13.55	76.70	30.29/0.8340	30.04/0.9014
	LN \rightarrow None, lr= 1×10^{-4}	238.37	13.55	76.70	30.15/0.8306	29.74/0.8970
	LN \rightarrow BN	239.52	13.72	76.70	30.28/0.8354	30.05/0.9029
	LN \rightarrow FBN*	238.37	13.55	76.70	30.30/0.8343	30.15/0.9028
	LN \rightarrow L ₂ normalization	238.37	13.55	76.70	30.39/0.8358	30.31/0.9049



(a) Effect of LayerNorm (b) Comparison of different normalizations

Figure 5. Smoothed training loss curves with or without normalization. Figure (a) shows LayerNorm stabilizes model training and converges better than without it. Figure (b) compares the effects of different normalization approaches on model training.

consumption and slower inference time. Thus, we use the CCM as the default channel mixer.

Effectiveness of the LayerNorm layer. Since we use the element-wise product in the SAFM module, it will result in abnormal gradient values and unstable model training, as shown in Figure 5(a). It is, therefore, necessary to normalize the input features. Here, we perform normalization with the LayerNorm [3] layer. To verify this assumption, we first remove the LayerNorm layer. Table 3 and Figure 5(a) suggest that without it, the model suffers a training crash at a large learning rate (i.e., 1×10^{-3}) and does not converge well at small ones (i.e., 1×10^{-4}) with its PSNR of only 30.15dB and 29.74dB on the DIV2K-val and Manga109

datasets, respectively. Next, we compare the LayerNorm with three representative normalization methods, including BatchNorm [21], Frozen BatchNorm (FBN) [21], and L₂ normalization in Figure 5(b). The results in Table 3 and Figure 5(b) demonstrate that the BN family decrease the PSNR/SSIM values by a large margin, and the FBN even does not guarantee a stable model training process. Although the L₂ normalization allows the model to be trained successfully, its performance is not as good as that of using LayerNorm. Thus, the LayerNorm layer is set as default for the proposed SAFMN.

6. Conclusion

In this paper, we propose a simple yet efficient deep CNN model to solve the efficient image super-resolution problem. The proposed SAFMN explores the long-range adaptability upon a multi-scale feature representation-based modulation mechanism. To complement the local contextual information, we further develop a compact convolutional channel mixer to encode spatially local context and conduct channel mixing simultaneously. We both qualitatively and quantitatively evaluate the proposed method on commonly used benchmarks. Experimental results show that the proposed SAFMN model is more efficient than state-of-the-art methods while achieving competitive performance.

References

- [1] Namhyuk Ahn, Byungkong Kang, and Kyung-Ah Sohn. Fast, accurate, and lightweight super-resolution with cascading residual network. In *ECCV*, 2018. 1, 2, 5, 6, 7
- [2] Pablo Arbeláez, Michael Maire, Charless C. Fowlkes, and Jitendra Malik. Contour detection and hierarchical image segmentation. *PAMI*, 33(5):898–916, 2011. 4
- [3] Jimmy Lei Ba, Jamie Ryan Kiros, and Geoffrey E. Hinton. Layer normalization. *arXiv preprint arXiv:1607.06450*, 2016. 4, 8
- [4] Marco Bevilacqua, Aline Roumy, Christine Guillemot, and Marie-Line Alberi Morel. Low-complexity single-image super-resolution based on nonnegative neighbor embedding. In *BMVC*, 2012. 1, 4
- [5] Hanting Chen, Yunhe Wang, Tianyu Guo, Chang Xu, Yiping Deng, Zhenhua Liu, Siwei Ma, Chunjing Xu, Chao Xu, and Wen Gao. Pre-trained image processing transformer. In *CVPR*, 2021. 1
- [6] Xiangxiang Chu, Bo Zhang, Hailong Ma, Ruijun Xu, and Qingyuan Li. Fast, accurate and lightweight super-resolution with neural architecture search. In *ICPR*, 2021. 1, 2
- [7] Xiaohan Ding, Xiangyu Zhang, Ningning Ma, Jungong Han, Guiguang Ding, and Jian Sun. Repvgg: Making vgg-style convnets great again. In *CVPR*, 2021. 2
- [8] Xiaohan Ding, Xiangyu Zhang, Yizhuang Zhou, Jungong Han, Guiguang Ding, and Jian Sun. Scaling up your kernels to 31x31: Revisiting large kernel design in cnns. In *CVPR*, 2022. 3
- [9] Chao Dong, Chen Change Loy, Kaiming He, and Xiaoou Tang. Image super-resolution using deep convolutional networks. *PAMI*, 38(2):295–307, 2016. 2, 5
- [10] Chao Dong, Chen Change Loy, and Xiaoou Tang. Accelerating the super-resolution convolutional neural network. In *ECCV*, 2016. 1, 2, 5
- [11] Alexey Dosovitskiy, Lucas Beyer, Alexander Kolesnikov, Dirk Weissenborn, Xiaohua Zhai, Thomas Unterthiner, Mostafa Dehghani, Matthias Minderer, Georg Heigold, Sylvain Gelly, Jakob Uszkoreit, and Neil Houlsby. An image is worth 16x16 words: Transformers for image recognition at scale. In *ICLR*, 2021. 1, 2, 3, 4, 7
- [12] Jinjin Gu and Chao Dong. Interpreting super-resolution networks with local attribution maps. In *CVPR*, 2021. 2
- [13] Meng-Hao Guo, Cheng-Ze Lu, Zheng-Ning Liu, Ming-Ming Cheng, and Shi-Min Hu. Visual attention network. *arXiv preprint arXiv:2202.09741*, 2022. 3
- [14] Kaiming He, Xiangyu Zhang, Shaoqing Ren, and Jian Sun. Deep residual learning for image recognition. In *CVPR*, 2016. 2
- [15] Zibin He, Tao Dai, Jian Lu, Yong Jiang, and Shu-Tao Xia. Fakd: Feature-affinity based knowledge distillation for efficient image super-resolution. In *ICIP*, 2020. 1, 2
- [16] Dan Hendrycks and Kevin Gimpel. Gaussian error linear units. *arXiv preprint arXiv:1606.08415*, 2016. 4, 7
- [17] Jie Hu, Li Shen, and Gang Sun. Squeeze-and-excitation networks. In *CVPR*, 2018. 4, 7
- [18] Jia-Bin Huang, Abhishek Singh, and Narendra Ahuja. Single image super-resolution from transformed self-exemplars. In *CVPR*, 2015. 4
- [19] Zheng Hui, Xinbo Gao, Yunchu Yang, and Xiumei Wang. Lightweight image super-resolution with information multi-distillation network. In *ACM MM*, 2019. 1, 2, 5, 6, 7
- [20] Andrey Ignatov, Radu Timofte, Maurizio Denna, and et al. Efficient and accurate quantized image super-resolution on Mobile NPUs, Mobile AI & AIM 2022 challenge: Report. In *ECCV Workshops*, 2022. 2
- [21] Sergey Ioffe and Christian Szegedy. Batch normalization: Accelerating deep network training by reducing internal covariate shift. In *ICML*, 2015. 2, 4, 8
- [22] Jiwon Kim, Jung Kwon Lee, and Kyoung Mu Lee. Deeply-recursive convolutional network for image super-resolution. In *CVPR*, 2016. 1
- [23] Jiwon Kim, Jung Kwon Lee, and Kyoung Mu Lee. Accurate image super-resolution using very deep convolutional networks. In *CVPR*, 2016. 2, 5, 6
- [24] Diederik P. Kingma and Jimmy Ba. Adam: A method for stochastic optimization. In *ICLR*, 2015. 5
- [25] Fangyuan Kong, Mingxi Li, Songwei Liu, Ding Liu, Jingwen He, Yang Bai, Fangmin Chen, and Lean Fu. Residual local feature network for efficient super-resolution. In *CVPR Workshops*, 2022. 1, 2
- [26] Wei-Sheng Lai, Jia-Bin Huang, Narendra Ahuja, and Ming-Hsuan Yang. Deep laplacian pyramid networks for fast and accurate super-resolution. In *CVPR*, 2017. 5, 6
- [27] Wenbo Li, Kun Zhou, Lu Qi, Nianjuan Jiang, Jiangbo Lu, and Jiaya Jia. LAPAR: Linearly-assembled pixel-adaptive regression network for single image super-resolution and beyond. In *NeurIPS*, 2020. 4, 5, 6, 7
- [28] Yawei Li, Kai Zhang, Luc Van Gool, Radu Timofte, et al. NTIRE 2022 challenge on efficient super-resolution: Methods and results. In *CVPR Workshops*, 2022. 3, 6
- [29] Zheyuan Li, Yingqi Liu, Xiangyu Chen, Haoming Cai, Jinjin Gu, Yu Qiao, and Chao Dong. Blueprint separable residual network for efficient image super-resolution. In *CVPR Workshops*, 2022. 1, 2
- [30] Jingyun Liang, Jiezhang Cao, Guolei Sun, Kai Zhang, Luc Van Gool, and Radu Timofte. SwinIR: Image restoration using swin transformer. In *ICCV Workshops*, 2021. 1, 2, 3, 4
- [31] Bee Lim, Sanghyun Son, Heewon Kim, Seungjun Nah, and Kyoung Mu Lee. Enhanced deep residual networks for single image super-resolution. In *CVPR Workshops*, 2017. 1, 2, 4, 5, 6, 7
- [32] Jie Liu, Jie Tang, and Gangshan Wu. Residual feature distillation network for lightweight image super-resolution. In *ECCV Workshops*, 2020. 1, 2
- [33] Ze Liu, Yutong Lin, Yue Cao, Han Hu, Yixuan Wei, Zheng Zhang, Stephen Lin, and Baining Guo. Swin Transformer: Hierarchical vision transformer using shifted windows. In *ICCV*, 2021. 2, 3, 4
- [34] Ilya Loshchilov and Frank Hutter. Sgdr: Stochastic gradient descent with warm restarts. In *ICLR*, 2017. 5
- [35] Yusuke Matsui, Kota Ito, Yuji Aramaki, Toshihiko Yamasaki, and Kiyoharu Aizawa. Sketch-based manga retrieval

- using manga109 dataset. *arXiv preprint arXiv:1510.04389*, 2015. 4, 7
- [36] Pablo Navarrete Michelini, Yunhua Lu, and Xingqun Jiang. edge-SR: Super-resolution for the masses. In *WACV, 2022*. 1, 2
- [37] Ilija Radosavovic, Raj Prateek Kosaraju, Ross Girshick, Kaiming He, and Piotr Dollar. Designing network design spaces. In *CVPR, 2020*. 6
- [38] Mark Sandler, Andrew Howard, Menglong Zhu, Andrey Zhmoginov, and Liang-Chieh Chen. MobileNetV2: Inverted residuals and linear bottlenecks. In *CVPR, 2018*. 4, 7
- [39] Wenzhe Shi, Jose Caballero, Ferenc Huszar, Johannes Totz, Andrew P. Aitken, Rob Bishop, Daniel Rueckert, and Zehan Wang. Real-time single image and video super-resolution using an efficient sub-pixel convolutional neural network. In *CVPR, 2016*. 2, 3, 5
- [40] Dehua Song, Chang Xu, Xu Jia, Yiyi Chen, Chunjing Xu, and Yunhe Wang. Efficient residual dense block search for image super-resolution. In *AAAI, 2020*. 1, 2
- [41] Long Sun, Jinshan Pan, and Jinhui Tang. ShuffleMixer: An efficient convnet for image super-resolution. In *NeurIPS, 2022*. 1, 2, 3, 4, 5, 6
- [42] Ying Tai, Jian Yang, and Xiaoming Liu. Image super-resolution via deep recursive residual network. *CVPR, 2017*. 1, 2
- [43] Mingxing Tan and Quoc Le. EfficientNetV2: Smaller models and faster training. In *ICML, 2021*. 2, 4, 7
- [44] Radu Timofte, Eirikur Agustsson, Luc Van Gool, Ming-Hsuan Yang, Lei Zhang, et al. NTIRE 2017 challenge on single image super-resolution: Methods and results. In *CVPR Workshops, 2017*. 4, 7
- [45] Longguang Wang, Xiaoyu Dong, Yingqian Wang, Xinyi Ying, Zaiping Lin, Wei An, and Yulan Guo. Exploring sparsity in image super-resolution for efficient inference. In *CVPR, 2021*. 5
- [46] Roman Zeyde, Michael Elad, and Matan Protter. On single image scale-up using sparse-representations. In *Curves and Surfaces, 2012*. 4
- [47] Kai Zhang, Martin Danelljan, Yawei Li, and et al. AIM 2020 challenge on efficient super-resolution: Methods and results. In *ECCV Workshops, 2020*. 6
- [48] Kai Zhang, Shuhang Gu, Radu Timofte, et al. AIM 2019 challenge on constrained super-resolution: Methods and results. In *ICCV Workshops, 2019*. 3, 6
- [49] Xindong Zhang, Hui Zeng, and Lei Zhang. Edge-oriented convolution block for real-time super resolution on mobile devices. In *ACM MM, 2021*. 1, 2, 5
- [50] Yulun Zhang, Kunpeng Li, Kai Li, Lichen Wang, Bineng Zhong, and Yun Fu. Image super-resolution using very deep residual channel attention networks. In *ECCV, 2018*. 1, 2
- [51] Hengyuan Zhao, Xiangtao Kong, Jingwen He, Yu Qiao, and Chao Dong. Efficient image super-resolution using pixel attention. In *ECCV Workshops, 2020*. 1, 2, 5

Spatially-Adaptive Feature Modulation for Efficient Image Super-Resolution - Supplemental Material -

Long Sun, Jiangxin Dong, Jinhui Tang, Jinshan Pan
Nanjing University of Science and Technology

Overview

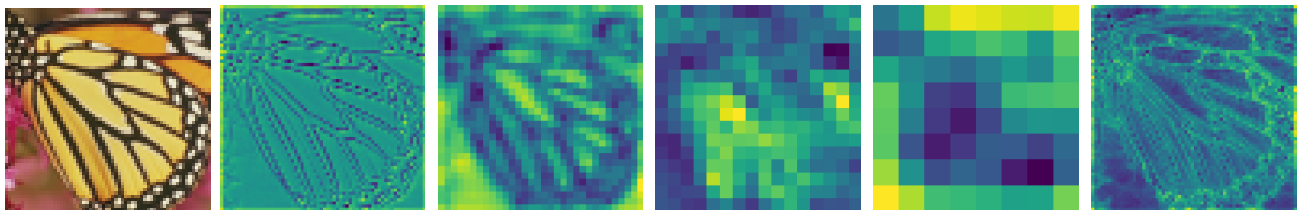
In this document, we further demonstrate the effectiveness of the proposed spatially-adaptive feature modulation and the LayerNorm layer in Section 1. Then, we evaluate our method with the challenge winners in Section 2. We further compare the proposed method with classic performance-oriented SR models in Section 3. Next, we make some notes on the Urban100 dataset in Section 4. Finally, we show more visual comparisons in Section 5.

1. Ablations of the spatially-adaptive feature modulation and the LayerNorm

Effect of scales in the spatially-adaptive feature modulation. We evaluate the effect of features at different scales in the spatially-adaptive feature modulation (SAFM) on the $\times 4$ DIV2K validation set. Table 1 shows that removing any scale information affects the reconstruction performance. We further show the visualization of learned features at different scales to better understand why the SAFM works. Figure 1 illustrates that the learned features are independent and complementary between scales, and aggregating these features helps grab the overall structure.

Effectiveness of the spatially-adaptive feature modulation. As described in the main paper, the proposed spatially-adaptive feature modulation layer consists of three components: feature modulation (FM), multi-scale representation (MR), and feature aggregation (FA). To intuitively illustrate what the SAFM block learns, we show some learned features in Figure 2, where the corresponding features are extracted before the upsampling layer. Figure 2 demonstrates that the deep features learned with SAFM layers contain much richer feature information and attend to more high-frequency details, facilitating the reconstruction of high-quality images.

Effectiveness of the LayerNorm layer. We show the visual results of different normalizations in Figure 3. As stated in the main paper, we obtained the results for the Frozen BatchNorm [5] and without the LayerNorm [2] before the training collapse. The model with BatchNorm layers generates images with unpleasant artifacts because it involves the estimated mean and variance of the entire training dataset during testing. The artifacts can be alleviated when we fix these estimates, as shown in Figure 3(c). Figure 3(d) and (f) show that applying normalization in the channel dimension can avoid the occurrence of artifacts. Compared to the L_2 normalization, the model with LayerNorm layers produces more precise results. We, therefore, introduce LayerNorm layers for stable training and well convergence. The reasons behind the LayerNorm remain to be further investigated.



(a) LR input

(b) Scale 1

(c) Scale 2

(d) Scale 4

(e) Scale 8

(f) Aggregated feature

Figure 1. Illustration of learned deep features from the SAFM at different scales.

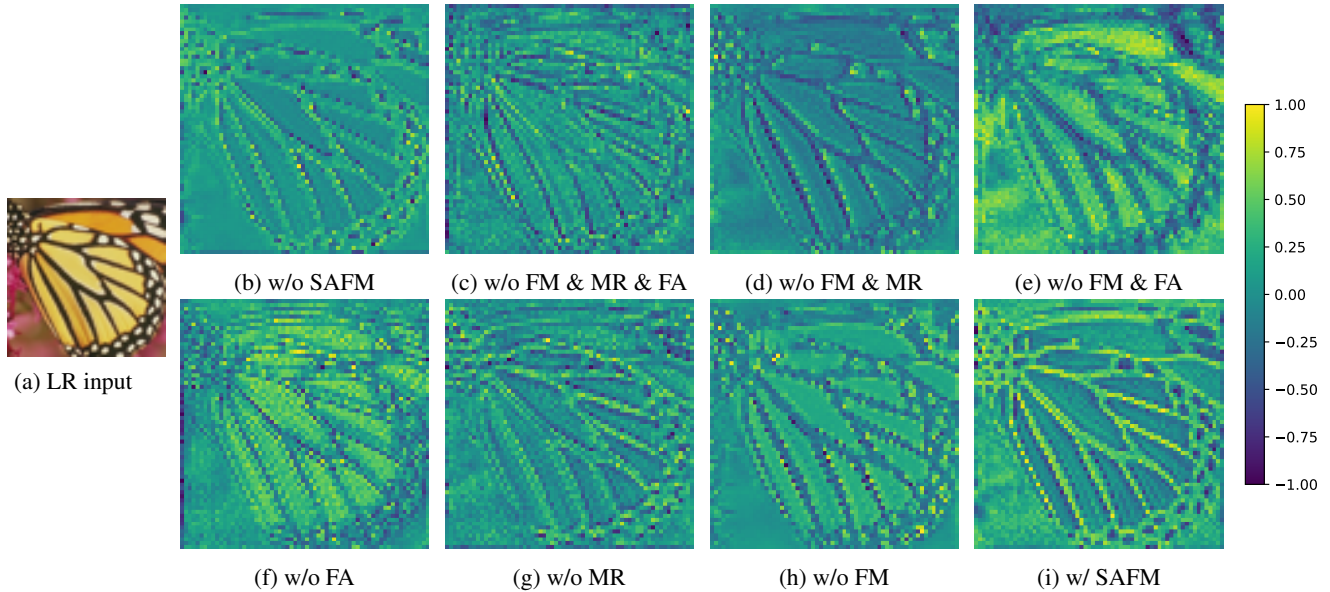


Figure 2. Illustration of learned deep features from the SAFM ablation. We average the features before the upsampling layer in the channel dimension and show the corresponding results. The proposed SAFM layer includes three components: feature modulation (FM), multi-scale representation (MR), and feature aggregation (FA). (h) indicates that the model pays less attention to the high-frequency regions without the feature modulation. (g) shows that the model fails to capture long-range information without the multi-scale representation. (f) illustrates the necessity of aggregating multi-scale features. The comparison of (i) with (b)-(h) suggests that the proposed method with the SAFM block yields a finer feature representation with clearer structures that pays more attention to high-frequency details.

Table 1. Effect of scales in the SAFM. We evaluate the effect of features at different scales in the SAFM on the $\times 4$ DIV2K validation set. The results show that removing any scale information affects the reconstruction performance.

Variants	SAFMN	w/o Scale 8	w/o Scale 8&4	w/o Scale 8&4&2
DIV2K_val	30.43/0.8372	30.39/0.8362	30.37/0.8357	30.34/0.8350

Table 2. Efficiency comparison with the challenge winners on $\times 4$ SR. #GPU Mem. and #Avg. Time denote the maximum GPU memory consumption and the average running time of the inference phase, respectively. #FLOPs, #Acts and #Avg. Time are computed on an LR image with a resolution of 320×180 pixels. Our SAFMN obtains comparable performance and a better trade-off between reconstruction performance and model complexity.

Methods	#Params [K]	#FLOPs [G]	#Acts [M]	#GPU Mem. [M]	#Avg. Time [ms]	B100 [PSNR/SSIM]
RFDN [13]	433.45	23.82	98.46	176.75	7.23	27.60/0.7368
RLFN [7]	543.74	29.88	111.17	145.69	7.35	27.60/0.7364
SAFMN	239.52	13.56	76.70	65.26	10.71	27.58/0.7359

2. Comparison with the challenge winners

We further compare our method with solutions of the challenge champion, i.e., RFDN (winner of AIM 2020 Efficient Super-Resolution Challenge [16]) and RLFN (winner of NTIRE 2022 Efficient Super-Resolution Challenge [10]). Table 2 demonstrates that our approach obtains a noticeable improvement in all measures except the running time. Table 3 shows that our slower running time is mainly due to the use of LayerNorm [2], which requires the mean and standard deviation of the input features in the inference phase. Without LayerNorm, the runtime improves to 8.35ms, which is very close to the speed of RLFN. As shown in Section 1, however, the importance of LayerNorm prevents us from removing this module directly. We will explore feasible alternatives in our further work. Moreover, we count the inference time of different commonly used tensor operations with the `torch.profiler` function to explicitly evaluate factors affecting the speed of our method. Table 3 presents that element-wise addition, element-wise product, and channel splitting are rather time-consuming. Since we use feature modulation and residual learning in each building block to learning high-frequency details, which also deteriorates the inference speed.

Table 3. GPU runtime of commonly used meta-operations on $\times 4$ SR. we count the time with the `torch.profiler` function.

Meta-operations	LayerNorm	Channel Splitting	Adaptive MaxPool	Nearest Interpolation	Element-wise Product	Element-wise Addition
Runtime [us]	465	133	85	24	156	193

Table 4. Comparison with classic SR models. #Params and #FLOPs are measured under the setting of upscaling SR images to 1280×720 pixels on all scales. The proposed SAFMN achieves comparable performances with significantly less computational and memory costs.

Scale	Methods	#Params [M]	#FLOPs [G]	Set5	Set14	B100	Urban100	Manga109
$\times 2$	EDSR [12]	40.73	9387	38.11/0.9602	33.92/0.9195	32.32/0.9013	32.93/0.9351	39.10/0.9773
	RCAN [17]	15.45	3530	38.27/0.9614	34.12/0.9216	32.41/0.9027	33.34/0.9384	39.44/0.9786
	SAN [3]	15.86	3050	38.31/0.9620	34.07/0.9213	32.42/0.9028	33.10/0.9370	39.32/0.9792
	HAN [14]	63.61	14551	38.27/0.9614	34.16/0.9217	32.41/0.9027	33.35/0.9385	39.46/0.9785
	SAFMN	5.56	1274	38.28/0.9616	34.14/0.9220	32.39/0.9024	33.06/0.9366	39.56/0.9790
	SwinIR [11]	11.75	2301	38.42/0.9623	34.46/0.9250	32.53/0.9041	33.81/0.9427	39.92/0.9797
$\times 3$	EDSR [12]	43.68	4470	34.65/0.9280	30.52/0.8462	29.25/0.8093	28.80/0.8653	34.17/0.9476
	RCAN [17]	15.63	1586	34.65/0.9280	30.52/0.8462	29.25/0.8093	28.80/0.8653	34.17/0.9476
	SAN [3]	15.90	1620	34.75/0.9300	30.59/0.8476	29.33/0.8112	28.93/0.8671	34.30/0.9494
	HAN [14]	64.35	6534	34.75/0.9299	30.67/0.8483	29.32/0.8110	29.10/0.8705	34.48/0.9500
	SAFMN	5.58	569	34.80/0.9301	30.68/0.8485	29.34/0.8110	28.99/0.8679	34.66/0.9504
	SwinIR [11]	11.94	1026	34.97/0.9318	30.93/0.8534	29.46/0.8145	29.75/0.8826	35.12/0.9537
$\times 4$	EDSR [12]	43.90	2895	32.46/0.8968	28.80/0.7876	27.71/0.7420	26.64/0.8033	31.02/0.9148
	RCAN [17]	15.59	918	32.63/0.9002	28.87/0.7889	27.77/0.7436	26.82/0.8087	31.22/0.9173
	SAN [3]	15.86	937	32.64/0.9003	28.92/0.7888	27.78/0.7436	26.79/0.8068	31.18/0.9169
	HAN [14]	64.20	3776	32.64/0.9002	28.90/0.7890	27.80/0.7442	26.85/0.8094	31.42/0.9177
	SAFMN	5.60	321	32.65/0.9005	28.96/0.7898	27.82/0.7440	26.81/0.8058	31.59/0.9192
	SwinIR [11]	11.90	834	32.92/0.9044	29.09/0.7950	27.92/0.7489	27.45/0.8254	32.03/0.9260

3. Comparison with classic SR models

To verify the scalability of SAFMN, we further compare the large version of SAFMN with the state-of-the-art classical SR methods, including EDSR [12], RCAN [17], SAN [3], HAN [14], SwinIR [11]. Table 4 shows that our SAFMN shows significant advantages in terms of model efficiency compared to the evaluated CNN-based methods and obtains competitive reconstruction performances, benefiting from its adaptability upon a multi-scale feature representation-based modulation mechanism.

4. Some notes on the Urban100 dataset

As shown in Table 5, the proposed SAFMN obtains a weak PSNR performance on the Urban100 dataset compared to other state-of-the-art methods, e.g., IMDN [4] and LAPAR-A [9]. The slight local luminance differences are responsible for these results. Since PSNR measures pixel-level distances rather than overall structure, slight differences in the luminance channel can lead to significant differences in PSNR. Furthermore, we visually compare images with a significant PSNR gap between our SAFMN and IMDN and observe no detectable changes in perceptual quality. Thus, we reevaluate these results using two commonly-used perceptual metrics: NIQE and LPIPS. Table 5 lists the quantitative results, and the proposed method achieves comparable performance to IMDN and LAPAR-A in terms of NIQE and LPIPS.

5. More visual results

In this section, we present additional visual comparisons with state-of-the-art methods [1, 4, 6, 8, 15] on the $\times 4$ Urban100 dataset. Figure 4 shows that the proposed algorithm generates clearer images with finer detailed structures than those by state-of-the-art methods.

References

- [1] Namhyuk Ahn, Byungkon Kang, and Kyung-Ah Sohn. Fast, accurate, and lightweight super-resolution with cascading residual network. In *ECCV*, 2018. 3, 6
- [2] Jimmy Lei Ba, Jamie Ryan Kiros, and Geoffrey E. Hinton. Layer normalization. *arXiv preprint arXiv:1607.06450*, 2016. 1, 2, 5
- [3] Tao Dai, Jianrui Cai, Yongbing Zhang, Shu-Tao Xia, and Lei Zhang. Second-order attention network for single image super-resolution. In *CVPR*, 2019. 3

Table 5. Quantitative comparison results on the Urban100 dataset. Our proposed method performs weakly in PSNR/SSIM but is comparable to IMDN and LAPAR in perceptual metrics, including NIQE and LPIPS.

Scale	Methods	#Params [K]	#FLOPs [G]	PSNR	SSIM	NIQE	LPIPS
×2	IMDN [4]	694	161	32.17	0.9283	4.59	0.1132
	LAPAR-A [9]	548	171	32.17	0.9250	4.55	0.1129
	SAFMN	228	52	31.84	0.9256	4.60	0.1138
×3	IMDN [4]	703	72	28.17	0.8519	5.21	0.2136
	LAPAR-A [9]	594	114	28.15	0.8523	5.21	0.2163
	SAFMN	233	23	27.95	0.8474	5.28	0.2134
×4	IMDN [4]	715	41	26.04	0.7838	5.69	0.2879
	LAPAR-A [9]	659	94	26.14	0.7871	5.63	0.2868
	SAFMN	240	14	25.97	0.7809	5.79	0.2881

- [4] Zheng Hui, Xinbo Gao, Yunchu Yang, and Xiumei Wang. Lightweight image super-resolution with information multi-distillation network. In *ACM MM*, 2019. 3, 4, 6
- [5] Sergey Ioffe and Christian Szegedy. Batch normalization: Accelerating deep network training by reducing internal covariate shift. In *ICML*, 2015. 1, 5
- [6] Jiwon Kim, Jung Kwon Lee, and Kyoung Mu Lee. Accurate image super-resolution using very deep convolutional networks. In *CVPR*, 2016. 3, 6
- [7] Fangyuan Kong, Mingxi Li, Songwei Liu, Ding Liu, Jingwen He, Yang Bai, Fangmin Chen, and Lean Fu. Residual local feature network for efficient super-resolution. In *CVPR Workshops*, 2022. 2
- [8] Wei-Sheng Lai, Jia-Bin Huang, Narendra Ahuja, and Ming-Hsuan Yang. Deep laplacian pyramid networks for fast and accurate super-resolution. In *CVPR*, 2017. 3, 6
- [9] Wenbo Li, Kun Zhou, Lu Qi, Nianjuan Jiang, Jiangbo Lu, and Jiaya Jia. LAPAR: Linearly-assembled pixel-adaptive regression network for single image super-resolution and beyond. In *NeurIPS*, 2020. 3, 4
- [10] Yawei Li, Kai Zhang, Luc Van Gool, Radu Timofte, et al. NTIRE 2022 challenge on efficient super-resolution: Methods and results. In *CVPR Workshops*, 2022. 2
- [11] Jingyun Liang, Jiezhong Cao, Guolei Sun, Kai Zhang, Luc Van Gool, and Radu Timofte. SwinIR: Image restoration using swin transformer. In *ICCV Workshops*, 2021. 3
- [12] Bee Lim, Sanghyun Son, Heewon Kim, Seungjun Nah, and Kyoung Mu Lee. Enhanced deep residual networks for single image super-resolution. In *CVPR Workshops*, 2017. 3
- [13] Jie Liu, Jie Tang, and Gangshan Wu. Residual feature distillation network for lightweight image super-resolution. In *ECCV Workshops*, 2020. 2
- [14] Ben Niu, Weilei Wen, Wenqi Ren, Xiangde Zhang, Lianping Yang, Shuzhen Wang, Kaihao Zhang, Xiaochun Cao, and Haifeng Shen. Single image super-resolution via a holistic attention network. In *ECCV*, 2020. 3
- [15] Long Sun, Jinshan Pan, and Jinhui Tang. ShuffleMixer: An efficient convnet for image super-resolution. In *NeurIPS*, 2022. 3, 6
- [16] Kai Zhang, Martin Danelljan, Yawei Li, and et al. AIM 2020 challenge on efficient super-resolution: Methods and results. In *ECCV Workshops*, 2020. 2
- [17] Yulun Zhang, Kunpeng Li, Kai Li, Lichen Wang, Bineng Zhong, and Yun Fu. Image super-resolution using very deep residual channel attention networks. In *ECCV*, 2018. 3



(a) GT

(b) BatchNorm [5]

(c) Frozen BatchNorm [5]



(d) L_2 normalization

(e) w/o LayerNorm [2]

(f) w/ LayerNorm [2]

Figure 3. Visual results of different normalization methods. The proposed model with LayerNorm layers reconstructs better images.

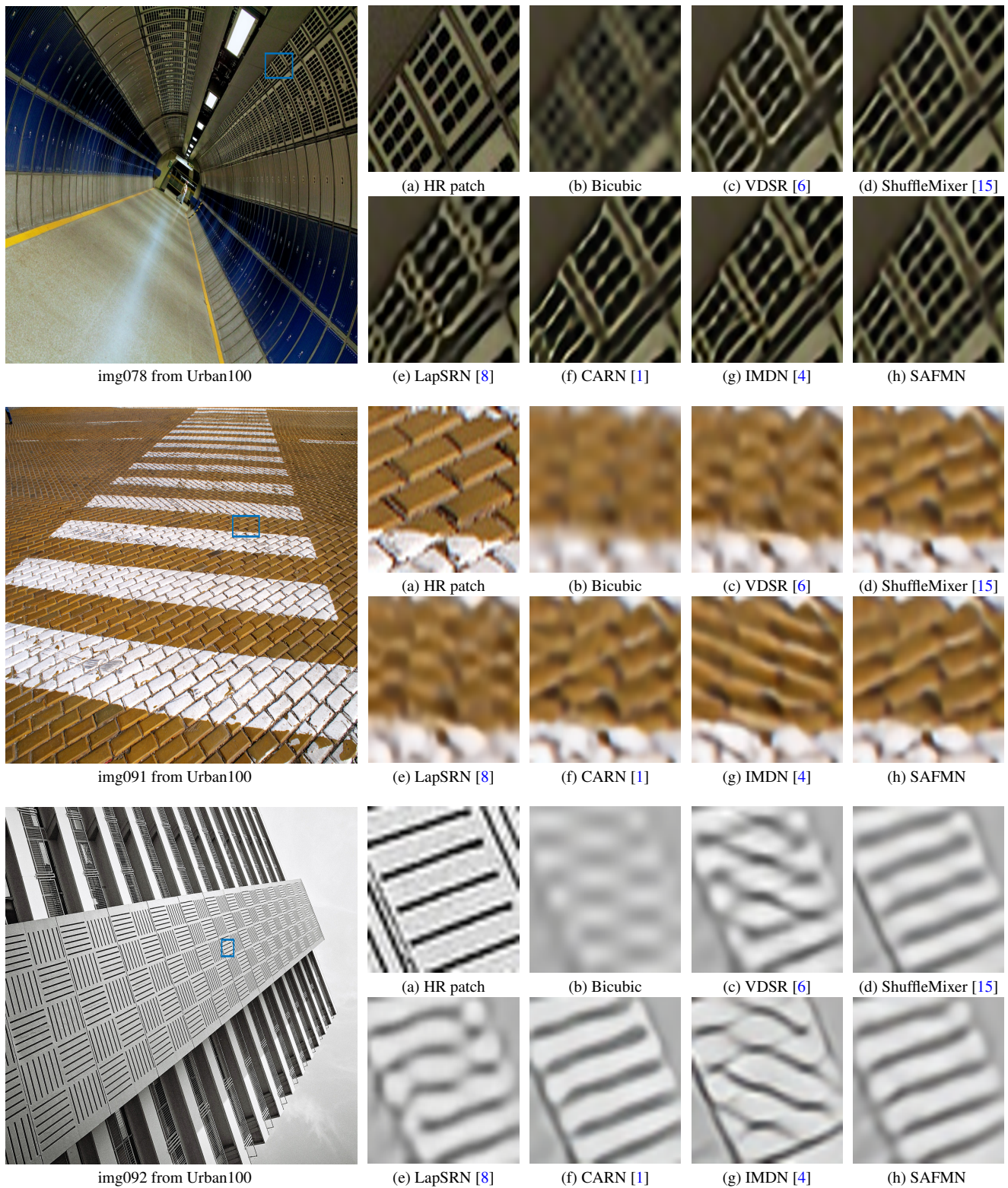


Figure 4. Visual comparisons for $\times 4$ SR on the Urban100 dataset. Our method generates images with clearer structures.